Structural basis of the signalling through a bacterial membrane receptor HasR deciphered by an integrative approach

Halina Wojtowicz*†[1], Ada Prochnicka-Chalufour*†[1], Gisele Cardoso de Amorim*†[2], Olga Roudenko‡, Catherine Simenel*†, Idir Malki*†, Gérard Pehau-Arnaudet†§, Francesca Gubellini†‖, Alexandros Koutsioubas¶, Javier Pérez‡, Philippe Delepelaire**, Muriel Delepierre*†, Rémi Fronzes*†‖ and Nadia Izadi-Pruneyre*†[3]

*Département de Biologie Structurale et Chimie, Unité de Résonance Magnétique Nucléaire des Biomolécules, Institut Pasteur, Paris, France
†CNRS, UMR 3528, Paris, France
‡Beamline SWING, Synchrotron SOLEIL, Saint-Aubin, France
§CITECH, Institut Pasteur, Paris, France
‖G5 Biologie Structurale de la Sécrétion Bactérienne, Institut Pasteur, Paris, France
¶Jülich Centre for Neutron Science, Forschungszentrum Jülich GmbH, Outstation at MLZ, Garching, Germany
**Institut de Biologie Physico-Chimique, CNRS Université Paris-Diderot, UMR 7099, Paris, France

Bacteria use diverse signalling pathways to adapt gene expression to external stimuli. In Gram-negative bacteria, the binding of scarce nutrients to membrane transporters triggers a signalling process that up-regulates the expression of genes of various functions, from uptake of nutrient to production of virulence factors. Although proteins involved in this process have been identified, signal transduction through this family of transporters is not well understood. In the present study, using an integrative approach (EM, SAXS, X-ray crystallography and NMR), we have studied the structure of the haem transporter HasR captured in two stages of the signalling process, i.e. before and after the arrival of signalling activators (haem and its carrier protein). We show for the first time that the HasR domain responsible for signal transfer: (i) is highly flexible in two stages of signalling; (ii) extends into the periplasm at approximately 70–90 Å (1 Å = 0.1 nm) from the HasR β-barrel; and (iii) exhibits local conformational changes in response to the arrival of signalling activators. These features would favour the signal transfer from HasR to its cytoplasmic membrane partners.

Key words: bacterial nutrient transporter, HasR, haem, integrative approach, *Serratia marcescens*, transmembrane signalling.

INTRODUCTION

Bacteria have developed a variety of strategies for adapting to their host environment and successfully colonizing it. One important mechanism of adaptation is the regulation of gene expression through the extracytoplasmic function σ factor (ECFσ), which responds to external stimuli. Some stimuli are scarce nutrients that are sensed by a family of transporters called TonB-dependent transporters. These transporters use for their activities the energy from the proton motive force of the cytoplasmic membrane, which is transduced by the TonB complex. The presence of a specific nutrient on the extracellular face of these transporters triggers a signal that activates the gene expression of various functions, from uptake of nutrient to production of virulence factors [1–4]. Although proteins involved in this signalling process have been identified, the mechanism of signal transduction through the TonB family of nutrient transporters is not well understood.

HasR is such a nutrient transporter with a signalling activity [5]. It belongs to the haem acquisition system (Has) developed by several Gram-negative bacteria to acquire haem as a source of iron [6]. In the present study, we focus on the Has system of *Serratia marcescens*, the first identified and intensely studied system [7]. HasR functions in synergy with HasA, a haem carrier protein. Extracellular haem, either free or bound to host haemoproteins, is captured by HasA, then delivered to the transporter, HasR, to be internalized [8]. The *has* operon which encodes the Has system proteins is regulated by the intracellular concentration of iron. Expression of Has system proteins commences under iron-deficient conditions, then increases when the appropriate iron source (haem and HasA) is detected on the extracellular side of the receptor [9]. The presence of these signalling activators is sensed by HasR and propagated through its periplasmic domain, called the signalling domain, to a cytoplasmic membrane anti-sigma factor and subsequently to the ECFσ factor, which activates the expression of the *has* operon. The signalling and transport activities of HasR require energy which is transduced by a specific TonB-like protein called HasB [10].

The atomic structure of HasR has so far been determined only for the receptor loaded with its external ligands, either HasA alone or HasA and haem [11]. In its loaded form, the HasR structure displayed the same overall fold as that observed in other TonB-dependent transporters. This structure comprised a membrane β-barrel, filled with a plug domain. The signalling domain (residues 1–85), responsible for signalling activity of HasR, was not visible in these X-ray structures probably due to the flexibility of the 27 residues (residues 86–112) that link the signalling domain

Abbreviations: CSP, chemical shift perturbation; DDM, *n*-dodecyl-β-D-maltopyranoside; ECFσ, extracytoplasmic function σ factor; FecA, ferric citrate transporter; Has, haem acquisition system; $HasR_{SD}$, fragment containing the signalling domain of HasR plus the linker; OM, outer membrane; SEC, size-exclusion chromatography; Zw, Zwittergent 3–14.

[1] These authors contributed equally to this work.

[2] Present address: Núcleo Multidisciplinar de Pesquisa UFRJ-Xerém, Divisão Biologia, Universidade Federal do Rio de Janeiro, Duque de Caxias, Rio de Janeiro, Brazil.

[3] To whom correspondence should be addressed (email nadia.izadi@pasteur.fr).

to the plug of the β-barrel. Interestingly, the linker contains the so-called HasB box, a crucial region that interacts with the energy transducer HasB [12]. The structure of the HasR signalling domain, like that of several other signalling domains, was solved in an isolated form by NMR, which revealed a conserved global fold [13–15].

The HasR signalling domain and the linker play a central role in this signalling by propagating the external signal from the transporter to its internal partners. The aim of the present study was to determine the structure, dynamics and positioning of the signalling domain in two stages of the process, i.e. before and after the arrival of signalling activators (haem and its carrier protein). To this end, we have studied the structure of two forms of HasR (free or loaded with its signalling activators), with an integrative approach combining the maps obtained by EM and distance distribution constraints derived from SAXS with high-resolution 3D structures of different subunits and sub-complexes.

The present study is the first to show that, in these two stages of the process, the signalling domain of HasR located in the periplasmic space is projected far from the barrel towards the cytoplasmic membrane. This position is the result of the high flexibility and the extension of the linker. Upon the arrival of signalling activators, the linker and the signalling domain undergo local conformational changes. We propose that these features provide substantial advantages for the signal transfer from HasR to its cytoplasmic membrane partners.

MATERIALS AND METHODS

Protein preparation

ΔNterHasR corresponds to the visible part of HasR in the X-ray structure of HasR–haem–HasA complex (PDB code 3CSL). This HasR mutant, lacking the 112 N-terminal residues (corresponding to the signalling domain plus the linker), was expressed with pFR2ΔNter plasmid constructed as follows. Two mutagenic oligonucleotides ΔNterHasR (5′-GCGGTAGCGCTCGCCAACGATTGGGTTTAC-3′) and ΔNterHasRr (5′-GTAAACCCAATCGTTGGCGAGCGCTACC-GC-3′) were used to mutate pFR2, by using the QuikChange kit from Stratagene. The mutation was verified by sequencing. A 338 bp EcoRI–NcoI fragment from the mutated plasmid was then reintroduced in an otherwise wild-type pFR2 digested with same enzymes to obtain pFR2ΔextTBB encoding ΔNterHasR.

All of the HasA samples used in the present study were His-tagged, prepared and purified as reported previously [16]. HoloHasA, the haem-loaded form of HasA, and $HasR_{SD}$ which comprised the signalling domain and the linker were prepared as previously described [17,18]. All HasB samples used in the present study corresponded to HasB C-terminal domain ($HasB_{CTD}$), with or without an N-terminal His-tag, and they were prepared as previously described [19,20].

HasR was purified as previously described with some modifications [8]. Solubilized membrane samples with 2 % and 2.5 % (w/v) of Zwittergent 3–14 (Zw; Anatrace) and containing HasR were loaded on an anion-exchange column (HiPrep Q HP 16/10, GE Healthcare Life Sciences) equilibrated and extensively washed with buffer A (0.1 M Tris-HCl, pH 7.5, and 0.08 % Zw). The bound proteins were then eluted with 20 column volumes that formed a linear gradient from buffer A to buffer B (0.1 M Tris-HCl, pH 7.5, 0.08 % Zw, and 1 M NaCl). Under these conditions, HasR was eluted with the 35 % gradient in a nearly pure form. The purest fractions were combined and concentrated to a maximum volume of 5 ml, then purified by size exclusion on a Sephacryl column (S-300 HP 26/60, GE Healthcare Life Sciences) equilibrated with 20 mM sodium phosphate buffer, pH 7, and 0.08 % Zw. All of the purification steps were performed at 4 °C or 12 °C in the presence of protease inhibitors (Roche Applied Sciences).

Protein concentrations were estimated using UV absorbance and the following calculated or determined molar absorption coefficients (21 350 $M^{-1}\cdot cm^{-1}$ at 276 nm for His–HasA; 140 000 $M^{-1}\cdot cm^{-1}$at 280 nm for HasR and 10 000 $M^{-1}\cdot cm^{-1}$ at 280 nm for HasB).

All HasR–haem–HasA wild-type or mutant complexes were prepared by adding an excess of HoloHasA to purified HasR/ΔNterHasR samples, followed by size-exclusion chromatography (SEC). In these complexes, as demonstrated in our previous studies, haem was transferred from HasA to HasR [8,11,12,21].

When required, we concentrated HasA or HasR samples in an Amicon Ultra centrifugal filter concentrator, with a 10 kDa or 100 kDa molecular mass cut-off respectively. A Superose 12 10/300 column (GE Healthcare Life Sciences) was used to exchange the buffer or detergent.

NMR spectroscopy

All NMR experiments were recorded at 20 °C on a Varian spectrometer operating at a proton frequency of 600 MHz and equipped with a cryogenically-cooled triple resonance $^{1}H\{^{13}C/^{15}N\}$ PFG probe. Experiments were run with the pulse sequences provided in the VnmrJ BioPack (Agilent Spinsights NMR & MRI Community, http://www.agilent.com/en-us/promotions/spinsights). NMR data were processed with NMRPipe/NMRDraw [22] and spectra were analysed with CcpNmr Analysis [23]. For NMR analysis of the HasR–haem–HasA complex, only HasR was ^{15}N-labelled. The ^{15}N HasR samples concentration ranged from 0.1 to 0.2 mM in 50 mM sodium phosphate buffer, pH 7.0, 0.04 % *n*-dodecyl-β-D-maltopyranoside (DDM; Anatrace) and 15 % $^{2}H_2O$. The HasR–haem–HasA NMR samples were prepared following two methods. In one method, unlabelled HoloHasA was mixed with labelled HasR and the complex was purified. In the other, aliquots of unlabelled HoloHasA were added to an NMR tube containing labelled HasR. The spectrum at the end of this titration was identical with that derived from the purified complex, which was used for the analyses. To prepare the complex of HasR–haem–HasA with HasB, lyophilized unlabelled HasB, at a concentration of 1.2 HasR equivalents, was directly added to the HasR–haem–HasA sample to avoid dilution. ^{15}N–^{1}H TROSY-HSQC and ^{15}N–^{1}H HSQC experiments were performed to analyse the HasR and the signalling domain samples respectively. Chemical shift perturbations (CSPs) of backbone ^{15}N–^{1}H resonances in the signalling domain of different HasR forms were calculated as previously described [12]. The analyses were performed with SAMPLEX [24]. The peak intensities were measured under CcpNmr Analysis [23].

The HasB–$HasR_{SD}$ interaction was investigated using ^{15}N–^{1}H HSQC spectra for different mixtures, where only one partner was ^{15}N-labelled. The experiments were recorded in 50 mM sodium phosphate buffer and 50 mM NaCl, pH 7.0, at 20 °C. The sample concentrations were 300 μM and 600 μM for the labelled and unlabelled partners respectively.

Negative stain EM

The small size of HasR complexes (<150 kDa) and the lack of symmetry made difficult the processing of cryo-EM data obtained for unstained low-contrast protein in vitreous ice and could not

really ensure the acquisition of higher resolution data. Therefore, we decided to adopt the negative stain strategy to visualize these complexes. At first, we visualized HasR with negative stain EM in the presence of detergent micelles. However, the free detergent micelles required to solubilize HasR gave rise to a low contrast image, which, in this case, was emphasized by the relatively low molecular mass of HasR (95 kDa). To overcome this problem, we replaced the detergent with amphipol A8-35, an amphipathic polymer that interacts with the hydrophobic surface of membrane proteins keeping them soluble [25]. Amphipol A8-35 binds nearly irreversibly to hydrophobic residues on protein; thus no free surfactant remains in solution.

Purified HasR and HasR–haem–HasA samples in 0.1 M Tris-HCl, 50 mM NaCl, pH 7.5, and 0.04 % DDM were mixed with amphipol A8-35 (Anatrace) at a 1:5 (w/w) ratio and incubated for 30 min at room temperature. After an additional 30 min of incubation with polystyrene beads at room temperature, the mixture was centrifuged and purified on a Superose 12 10/300 column equilibrated with 0.1 M Tris-HCl, 50 mM NaCl, pH 7.5. The sample was diluted with the same buffer to an optimal concentration for EM (approximately 0.4 μM, based on serial dilution tests). Aliquots (5 μl) were applied to a carbon-coated grid that had been glow discharged (5 mA/15 s/3 $\times$ 10^{-1} mbar; 1 bar = 100 kPa) with Quorum Q150 RES 15 min prior to sample application. After a 30 s incubation, the protein sample was blotted with filter paper, and the grid was washed twice with 50 μl drops of Milli-Q water for 10 s. The excess Milli-Q water was removed, and protein was negatively stained for 2 min with 2 % (w/v) uranyl acetate.

Micrographs were collected with a FEI Falcon II camera (4000 pixels $\times$ 4000 pixels) in a FEI Tecnai F20 electron microscope operated at 200 kV, which resulted in a pixel size of 2.0 Å (1 Å = 0.1 nm). Data were automatically collected with EPU software at defocus values between 0.4–2.5 μm.

EM data processing and 3D reconstruction

Only images that lacked both astigmatism and drift were processed. Particles were selected with the EMAN2.1 [26] Boxer routine within boxes of 160 pixels $\times$ 160 pixels. After the contrast transfer function estimation and correction with phase flipping (EMAN2.1: e2ctf), two sets of 117 712 and 90 231 particles were generated for the free HasR and the HasR–haem–HasA complex respectively. Further analysis, including 2D and 3D classifications and refinements, were performed with RELION1.3 [27,28]. Three rounds of the reference-free 2D class averaging were performed to clean up the two datasets. Final datasets of 21 409 particles for free HasR and 41 590 particles for the complex were submitted to 3D classifications with three and four classes respectively. 3D electron density maps with a resolution of 20 Å and the same pixel and box sizes as the datasets were calculated for the structures of the free HasR and the HasR–haem–HasA complex (PDB code 3CSL) with a corona of surfactant covering their membrane embedded part. As for the free form, the barrel and plug domains of HasR were taken from the X-ray structure of the complex. The corona was modelled, based on the SAXS data (see below), under the assumption that the covering surfaces of amphipol A8-35 and detergent were similar, as reported previously [29,30]. These calculated maps were used as references in the 3D classification procedures. Of note, the HasR signalling domain was not visible in the X-ray structure, therefore its absence in the references prevented a possible bias towards solutions with a particular localization for this domain. Finally, the RELION auto-refine procedure, with no imposed symmetry, was carried out with 14 158 and 9171 particles for our two samples. The refined maps were obtained with a resolution of 23 Å (according to the gold standard criterion of a Fourier shell correlation of 0.143 implemented in RELION). RELION post-processing was then applied to the final reconstructions, and the masked maps obtained at this stage were later used for visualization and model construction with UCSF Chimera software [31]. Chimera's fitting procedures were used for docking the available atomic structures of the barrel domains in free HasR or in HasR–haem–HasA into the EM maps. The NMR solution structure of the signalling domain alone (PDB code 2M5J) was positioned interactively. The conformations of residues 86–112 corresponding to the linker between the folded part of the signalling domain and the plug of HasR, were generated with the Modeller [32] program interfaced to Chimera.

SAXS

Details on the SAXS experiments and data collection methods are described in the Supplementary Experimental Procedures and Figure S1. Briefly, we employed a combination of SEC–HPLC with SAXS to obtain pure scattering curves from the protein–detergent complexes, devoid of parasitic scattering that arose from free detergent micelles or other constituents in the solution.

The detergent molecules that formed a corona around HasR contributed to the SAXS signal. To model this corona, we used SAXS data from the analysis of ΔNterHasR–haem–HasA. This mutant complex corresponded to the visible part of the X-ray structure (PDB code 3CSL). The SAXS data from the protein–detergent complex were fitted with the methodology previously used for the DDM-solubilized Aquaporin-0 protein [33]. Given the X-ray structure of HasR–haem–HasA, a hollow toroidal detergent belt was built around the transmembrane surface composed of two different phases: the inner hydrophobic part and the outer hydrophilic part of the detergent. The program Memprot [34] was used to find the detergent belt parameters (the height = a, the cross-sectional minor and major axes = b/e and the variable, be, where e is the ellipticity of the torus). The program found parameter values that best and accurately fitted the experimental curve (Supplementary Figures S3 and S4). In contrast with the calculation for Aquaporin-0, which had a symmetrical transmembrane profile, the ΔNterHasR–haem–HasA complexd could only be fitted well when the parameter b, which defined the axial dimensions of the toroidal cross-section, was locally modified to take into account the large asymmetry of the protein's transmembrane profile. In this refined approach, the protein asymmetry was mimicked on to the form of the constructed detergent belts, as expected intuitively (Supplementary Figures S3 and S4).

The SAXS-based refinement of the signalling domain position was performed with DADIMODO [35], which implemented a stochastic optimization procedure that called CRYSOL [36], to simulate SAXS curves and MMTK [37], to constrain the energy terms of candidate structures to values below a reasonable threshold, during the optimization process. This unusual model required that DADIMODO had to deal with the PDB file of a membrane protein–detergent complex, which included both an all-atom description of the protein moiety and a coarse-grain representation of the detergent corona. Therefore, its code was enriched with a mechanism that allowed it to work with the two coexisting representations. This enhancement was designed for instances where CRYSOL and MMTK did not interpret some modelling novelties in the same way (such as the PDB format of the detergent belt model in the present study).

DADIMODO relies on a genetic algorithm, where the fitness of every single structure within a 'population' of 20 individuals

is evaluated at each iteration; this approach can potentially lead to global optimization and avoid local minima traps. The fitness is directly equal to the χ^2 value provided by CRYSOL, which monitors the disagreement between the SAXS experimental data and the model curve. To ensure a truly efficient exploration of the conformational space, the population size has to be sufficiently large. For the present study, we benefited from the latest DADIMODO version, which performed the evaluations (SAXS curve simulation and calculation of the energy terms) for all of the structures at each iteration in parallel. Then, when it was executed on the Soleil cluster, it could evaluate up to 20 structures as rapidly as it evaluated one structure. This considerable increase in speed made it possible to perform dozens of high-quality runs for each of the two cases, HasR–haem–HasA and HasR. The structures that best fitted the SAXS experimental curves are presented and discussed. The DADIMODO optimization procedure is not highly sensitive to the choice of the starting structure, primarily because the starting population is generated with strong randomization to ensure sufficient variety for the search procedure. Each of 20 structures was obtained by randomly modifying the (φ,Ψ) backbone torsion angles, based on ten randomly chosen linker residues, then the fitness was computed. However, the feasibility of the structure, in terms of stereochemical restraints, was controlled after every rotation. The degrees of freedom used in the SAXS data fitting procedure were the (φ,Ψ) backbone torsion angles of the residues in the linker (86–112).

RESULTS

Behaviour of the signalling domain and the linker in whole HasR at two different stages of the signalling

Recently, we used NMR to solve the structure of $HasR_{SD}$, a fragment that comprised the first 112 residues (11 kDa) of HasR, namely its signalling domain and linker [15]. To find out whether that structure was conserved in the context of the full-length transporter, we analysed the ^{15}N–^{1}H HSQC spectrum of the free form of HasR. The detection of interpretable NMR signals from proteins of such a size (95 kDa plus approximately 50 kDa of detergent corona) is a challenge, due to their long overall rotational correlation time. However, we reasoned that it might be possible to detect NMR signals from some of the more dynamic parts of the transporter. Surprisingly, the ^{15}N–^{1}H HSQC spectrum of the full-length HasR appeared to be nearly identical with that of $HasR_{SD}$ (Figure 1A). The only additional visible resonances correspond to the amino groups of glutamine and asparagine residues (between 6.5–8 ppm), which have highly flexible side chains. The fact that only the resonances of the signalling domain and of the linker are visible indicates that their overall tumbling rate is shorter than that of the remaining parts of HasR, including extracellular loops and periplasmic turns.

We could readily assign all ^{15}N–^{1}H backbone resonances of the signalling domain and of the linker, based on the assignments made for $HasR_{SD}$. Only the last three residues of the linker (110–112) could not be assigned. Consequently, the overall 3D structures of the signalling domain and the linker are conserved, when these regions are attached to HasR.

To determine whether the structures of these parts of HasR were modified upon the arrival of the signalling activators, we compared the HSQC spectra of the free HasR and the HasR loaded with HasA and haem (HasR–haem–HasA) (Figure 1B). These spectra are highly similar. The signalling domains and the linkers in these two forms of HasR show conserved structure, with their own dynamics, and they behave as independent domains that lack a stable interaction with the β-barrel.

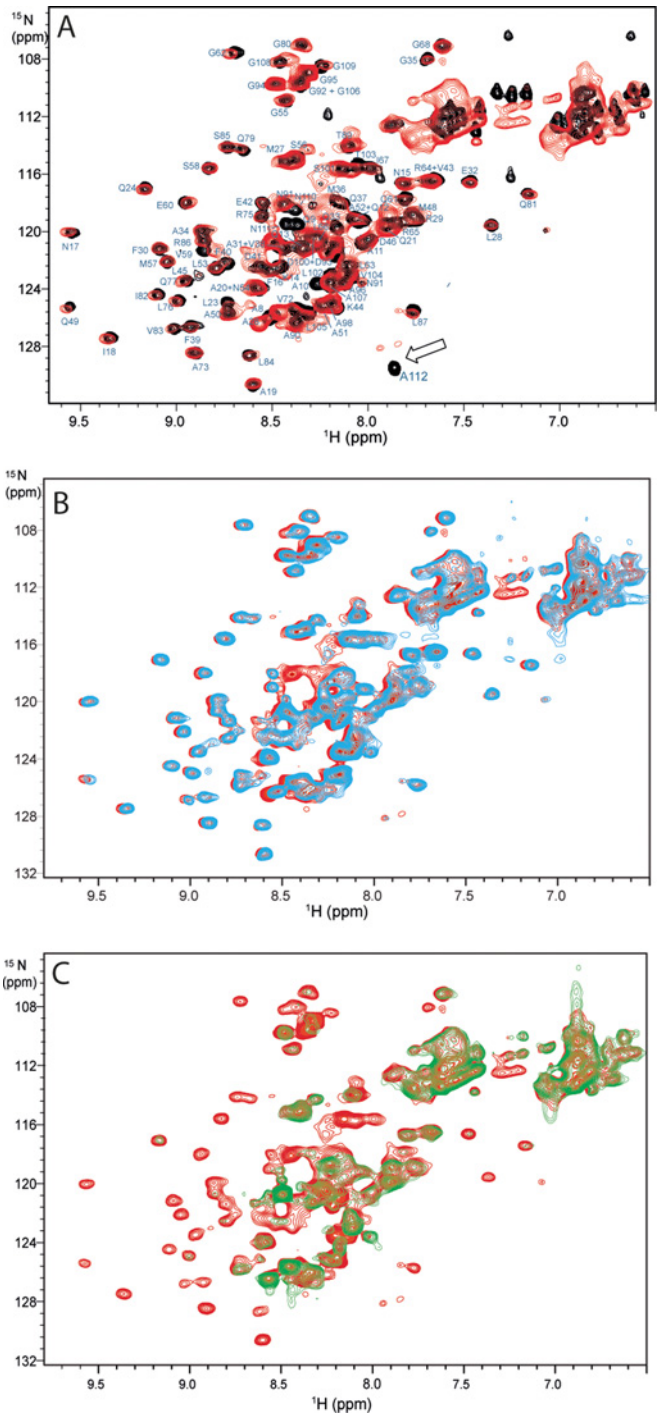

Figure 1 NMR analysis of different states of the HasR transporter

The ^{15}N–^{1}H HSQC spectra data show (**A**) the full-length HasR (red) superimposed on $HasR_{SD}$ [black in (**A**)] corresponding to a fragment comprising the signalling domain and the linker; (**B**) the HasR–haem–HasA complex (blue) superimposed on HasR (red); and (**C**) the (HasR–haem–HasA + HasB) complex (green) superimposed on HasR (red). Resonance assignments are indicated in blue (**A**). The last C-terminus residue of $HasR_{SD}$ is indicated with an arrow (**A**).

Structural features of HasR at two different stages of signalling

To obtain 3D reconstructions of HasR in its free and loaded forms, we combined the maps of HasR determined by negative stain EM and the constraints provided by SAXS with the known 3D structures of different portions of the transporter (the barrel, plug

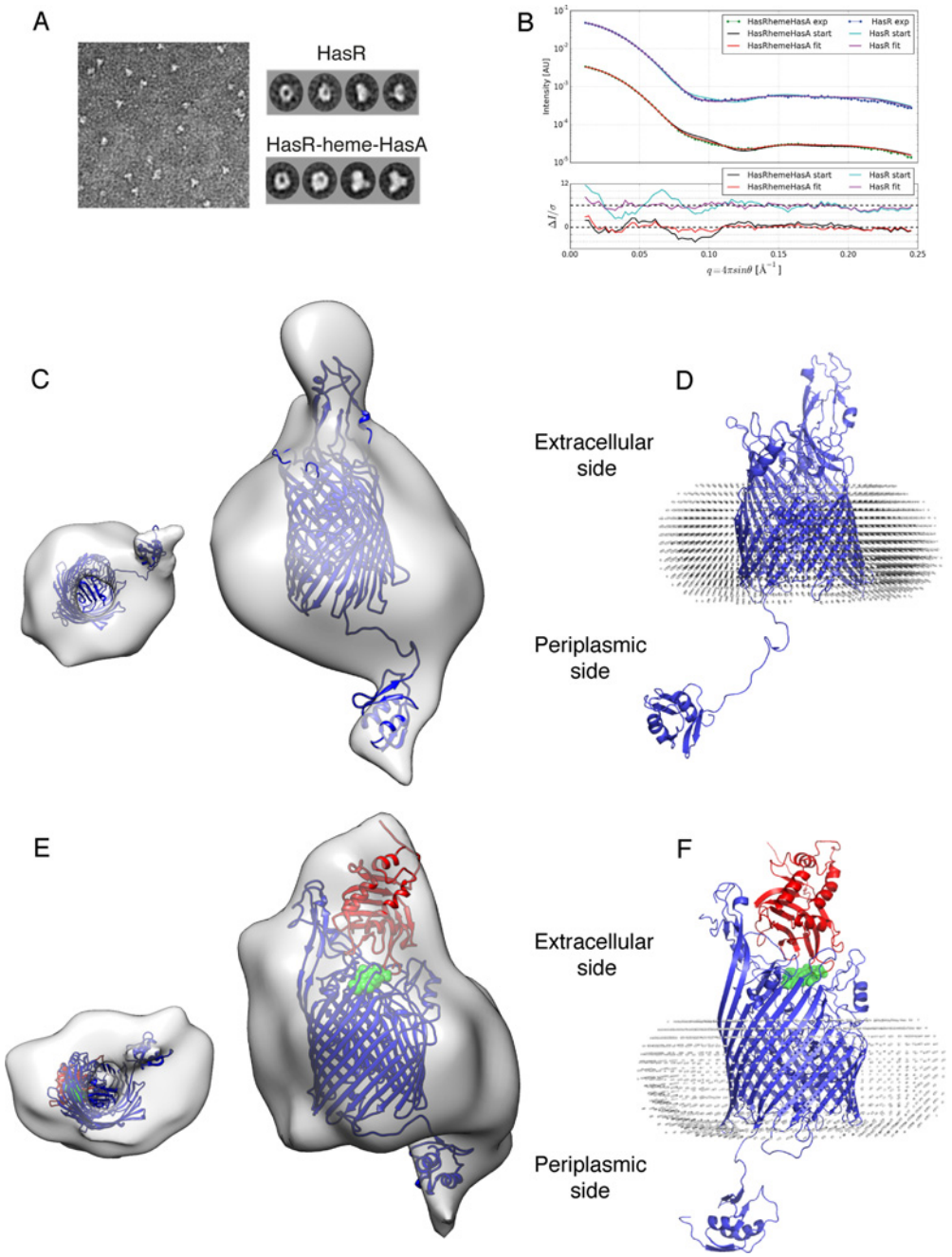

Figure 2 Results of EM and SAXS experiments

(**A**) Left: EM micrograph shows various orientations of the particles that comprise HasR–haem–HasA complexes. Right: representative class 2D averages for HasR and the complex, as indicated; (**B**) Upper panel: comparison of the experimental signal intensities (exp) and the simulated SAXS curves (start, fit) that were fitted to the starting and refined structures. Lower panel: the difference between the experimental and simulated intensities over the experimental σ values for starting (start) and optimized (fit) structures. The curves that correspond to HasR–haem–HasA and HasR experiments are shifted for clarity. (**C**) EM 3D reconstruction of HasR in its free form Left: viewed from the periplasmic side through the pore. Right: viewed from the side, with the extracellular side on top. (**D**) SAXS-derived model of HasR in its free form. (**E**) EM 3D reconstruction and (**F**) SAXS-derived model of the HasR–haem–HasA complex. HasA: red, haem: green, HasR: blue, detergent molecules in (**D**) and (**F**): grey, EM map: translucent grey. The same orientation of the barrel is represented in (**C**) and (**D**) and (**E**) and (**F**).

and signalling domains) and that of its ligands (haem and HasA) (Figure 2).

In negative stain EM, HasR samples produce high-contrast images. Particles, approximately 10 nm long, are homogeneously distributed in various orientations (Figure 2A).

The EM map obtained for the free HasR matches the shapes of the HasR barrel and plug domains derived from the X-ray structure of the HasR–haem–HasA complex, where the signalling domain is not observed (Figure 2C) [11]. The long extracellular loops of HasR, which correspond to the HasA-binding site can be readily identified. The channel inside the barrel, partially occluded by the plug (periplasmic view) is particularly well resolved. The visibility of this detail in such a small assembly subjected to single particle analysis with negative stain was unexpected.

At the periplasmic side of the transporter, an additional density is visible that matches the shape and the size of the signalling

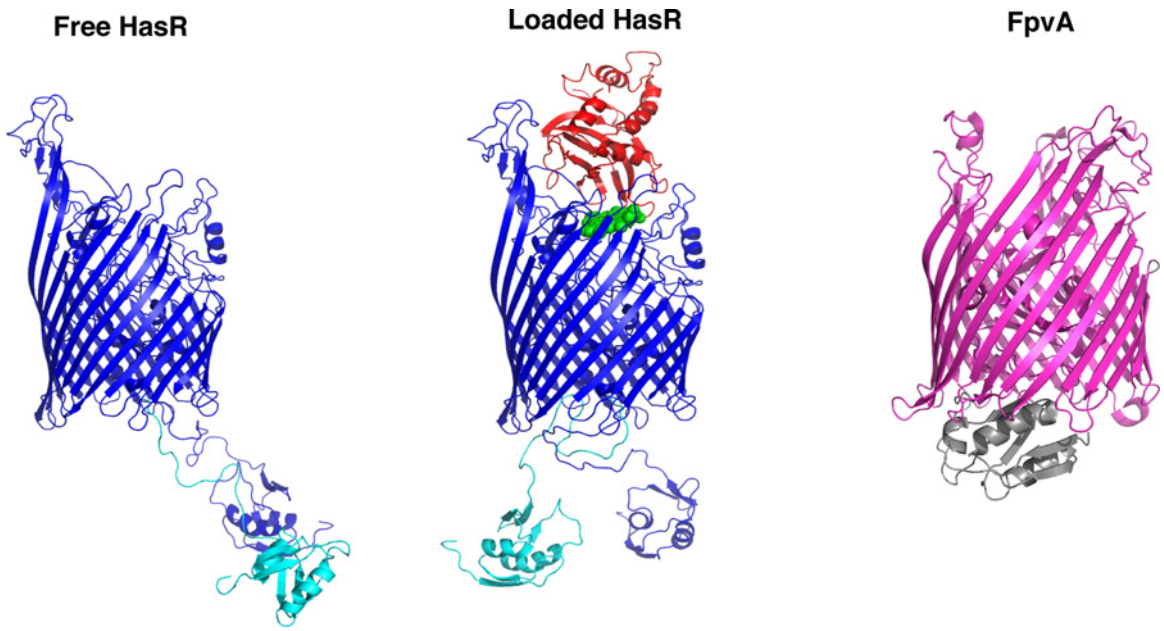

Figure 3 Signalling domain position in different transporters

The free HasR (left), the loaded HasR or the HasR–haem–HasA complex (middle) and FpvA (right) (PDB code 2O5P) with its signalling domain in grey. The 3D reconstructions of HasR from EM maps are in dark blue, SAXS-derived models are in cyan, HasA is in red and haem is in green. To simplify, only one β-barrel is shown.

domain [15]. The signalling domain is distant from the barrel. The distance (centroid to centroid) between the globular part of the signalling domain and the β-barrel is 80 Å.

The SAXS measurements were acquired online during elution of the protein sample from a gel-filtration column. This technique enabled analysis of a homogeneous HasR/detergent sample, without aggregated proteins or free detergent micelles (Supplementary Figure S1). In a first step, the detergent corona was modelled based on the methodology developed at Synchrotron Soleil [34], using the ΔNterHasR–haem–HasA complex mutant corresponding to the visible parts of the X-ray structure of HasR–haem–HasA [11]. In a second step, the conformation of the linker and the position of the signalling domain were optimized, using the program DADIMODO [35] specially upgraded to account for the coarse-grain model of the corona. The model thus derived (Figures 2B and 2D) for free HasR represents the average temporal and spatial distance distributions of molecules in solution. In this model (Figure 2D), the signalling domain is on average located at 90 Å from the β-barrel in the periplasmic space.

Our EM map of HasR–haem–HasA corresponds well to the known crystal structure in which the HasR signalling domain and the linker are missing. Nevertheless, as in the case of the free HasR, the EM map displays an additional electron density that could accommodate the solution structure of the HasR signalling domain (Figure 2E) [15]. The 3D reconstruction of the full-length HasR in complex with its signalling activators shows that the signalling domain remains at 70 Å from the barrel. In the model derived from the SAXS data, the signalling domain is located at approximately 70 Å from the barrel, and its position is very similar to that found with EM (Figures 2F and 3). Although the distance between the signalling domain and the barrel is comparable in both the EM and SAXS-derived structures, the location of the signalling domain with respect to the barrel axis differs (Figure 3); this might be due to the different sensitivities of the two methods to averaged ensemble conformations.

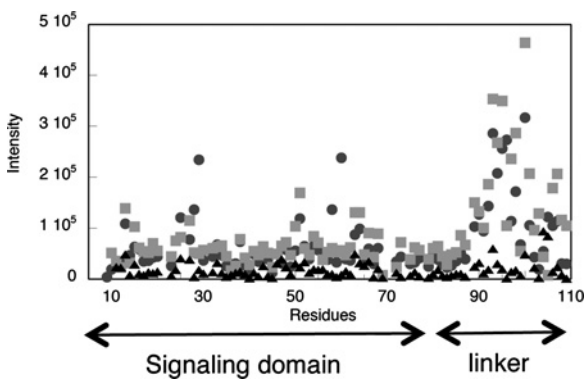

Figure 4 NMR signal intensities for the different HasR forms

The peak intensities on ^{15}N–^{1}H HSQC spectra are shown for HasR in its free form (circles), its loaded form, HasR–haem–HasA (squares), and the (HasR–haem–HasA + HasB) complex (triangles).

Conformational changes in the signalling domain and linker upon the arrival of signalling activators

To determine whether the presence of signalling activators on the extracellular side of HasR triggers local structural and dynamic changes in the signalling domain and in the linker, we analysed the ^{15}N–^{1}H HSQC spectra of different forms of HasR.

In the free form, the intensities of signals corresponding to the linker region are higher than those observed for the signalling domain. This difference in signal intensity indicates that the linker has a higher flexibility than the signalling domain (Figure 4).

When HasR is loaded with signalling activators, it presents the same general behaviour as it does in the free form (Figures 1A and 1B). However, the chemical shifts are modified in some stretches of residues, including: several residues in the first helix, H1 [25–37], a few residues in helix H2 (64–69) facing H1 and

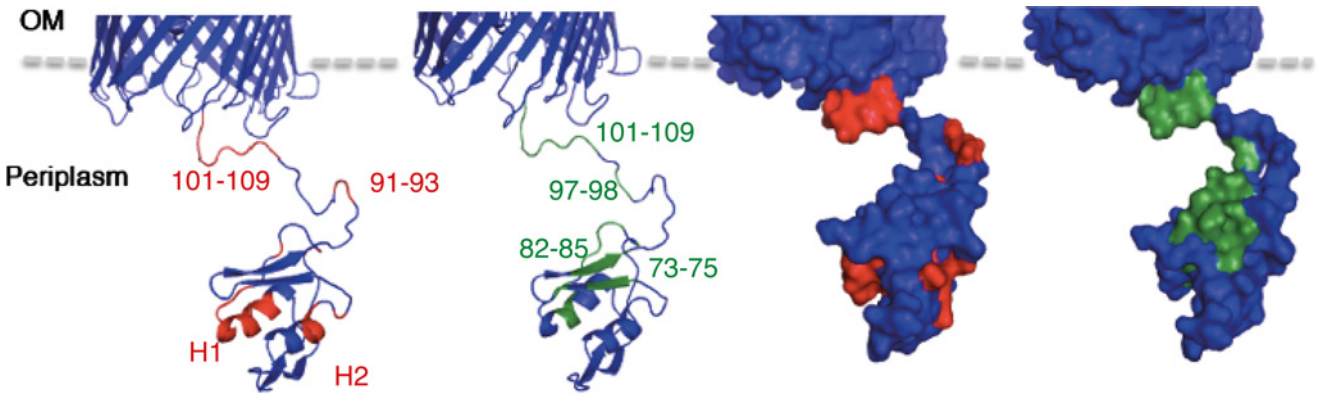

Figure 5 CSPs mapped on to HasR linker and signalling domain structures

The two ribbon structures on the left are shown in surface representation on the right. Each pair shows residues that were highly affected by the presence of the signalling activators (haem and HasA) (red; left panels) and those affected by the presence of HasB (green; right panels).

several residues in the linker (91–93 and 101–109) (Figure 5 and Supplementary Figure S2).

HasB effect on the structure and dynamics of the signalling domain

The linker harbours the HasB box, the main region of interaction between HasR and HasB. Using NMR, we monitored this interaction by adding HasB to the HasR–haem–HasA complex. The first observation was that the intensity decreased dramatically in all detected resonances that belonged to the signalling domain and the linker (Figure 4). This effect can be due to a change in the dynamics of these regions and/or to conformational exchange between different states (for example free and bound). The linker which appeared more flexible in the absence of HasB (more intense signals) exhibits a more significant reduction in signal intensity than the globular region. In fact, in the presence of HasB, these two regions display similar signal intensities and they adopt the same overall rotational correlation time, most likely due to the interaction between HasR and HasB (Figure 4). Despite the decrease in signal intensity, we could compare the chemical shifts in residues located in the signalling domain and the linker, in the context of the whole HasR, before and after the addition of HasB. That analysis showed that, in addition to residues in the linker region (97, 98 and 101–109), the presence of HasB significantly affected residues in the β-sheet located upstream of the linker (residues 73–75, 77 and 82–85) (Figure 5). These chemical shift variations could be due to either direct interaction between these residues and HasB or to a long-distance effect.

To gain more information about the HasB–HasR interaction, we investigated the interaction between HasB and $HasR_{SD}$ by NMR (Figure 6). The ^{15}N–^{1}H signals of both partners change due to the formation of a complex. On the HasB side, the signals corresponding to the third β-strand (120–126) disappear and are not replaced by any new peak. Residues of this strand undergo conformational changes occurring on the micro- to milli-second time scale upon the complex formation. Given these conformational changes and the low affinity of the complex [K_d approximately 400 μM estimated by surface plasmon resonance (SPR), results not shown], we could not detect signals corresponding to intermolecular constraints. Other residues of HasB showing large CSPs include the first β-strand (64, 66 and 69) and the helices (H1, H2 and H3) that surround the β-sheet (Figure 6) [12]. All these residues affected in HasB are identical with those modified in a previous study upon the interaction with a peptide corresponding to the linker [12]. In that study, we showed that the linker peptide formed an inter-protein β-sheet with the third β-strand of HasB. Now, on the $HasR_{SD}$ side, the residues most affected by the presence of HasB are those of the linker (101–111) (Figure 6). All of the spectral modifications observed in the present study suggest a similar formation of an inter-protein β-sheet between HasB and $HasR_{SD}$.

DISCUSSION

In the present study, we show using NMR that the structure of the signalling domain is conserved in the context of the whole transporter HasR, in both its free and its loaded (HasR–haem–HasA) forms, which correspond to two different stages of the signalling process. Furthermore, the linker connecting the signalling domain to the barrel is disordered and highly dynamic, maintaining the signalling domain away from the outer membrane (OM). These data show also that the signalling domain behaves as an independent domain with its own dynamics without any stable interaction with the rest of the transporter, but give no clues as to its position with respect to the barrel.

In a further step, in order to determine the position, so far unknown, of the signalling domain in the context of the whole HasR, we have used an integrative approach to obtain the overall structure of the HasR transporter in its free and loaded forms. The EM experiments provided a large number of particles which pointed to a unique positioning of the signalling domain, representing either the major conformation of the receptor or a unique one stabilized by our experimental conditions. The same overall structures and the signalling domain positions are obtained in the SAXS-derived structures, though they represent the average of the conformations coexisting in solution. This similarity between the results obtained by two independent techniques and modelling approaches reinforces their relevance.

The present study reveals structural features which have never been reported or predicted so far for a TonB-dependent transporter [38,39]. First, in both free and loaded forms, the signalling domain is located far from the barrel of HasR (at 70–90 Å) and directed towards the cytoplasmic membrane. The only known structure of a TonB-dependent transporter with a visible signalling domain

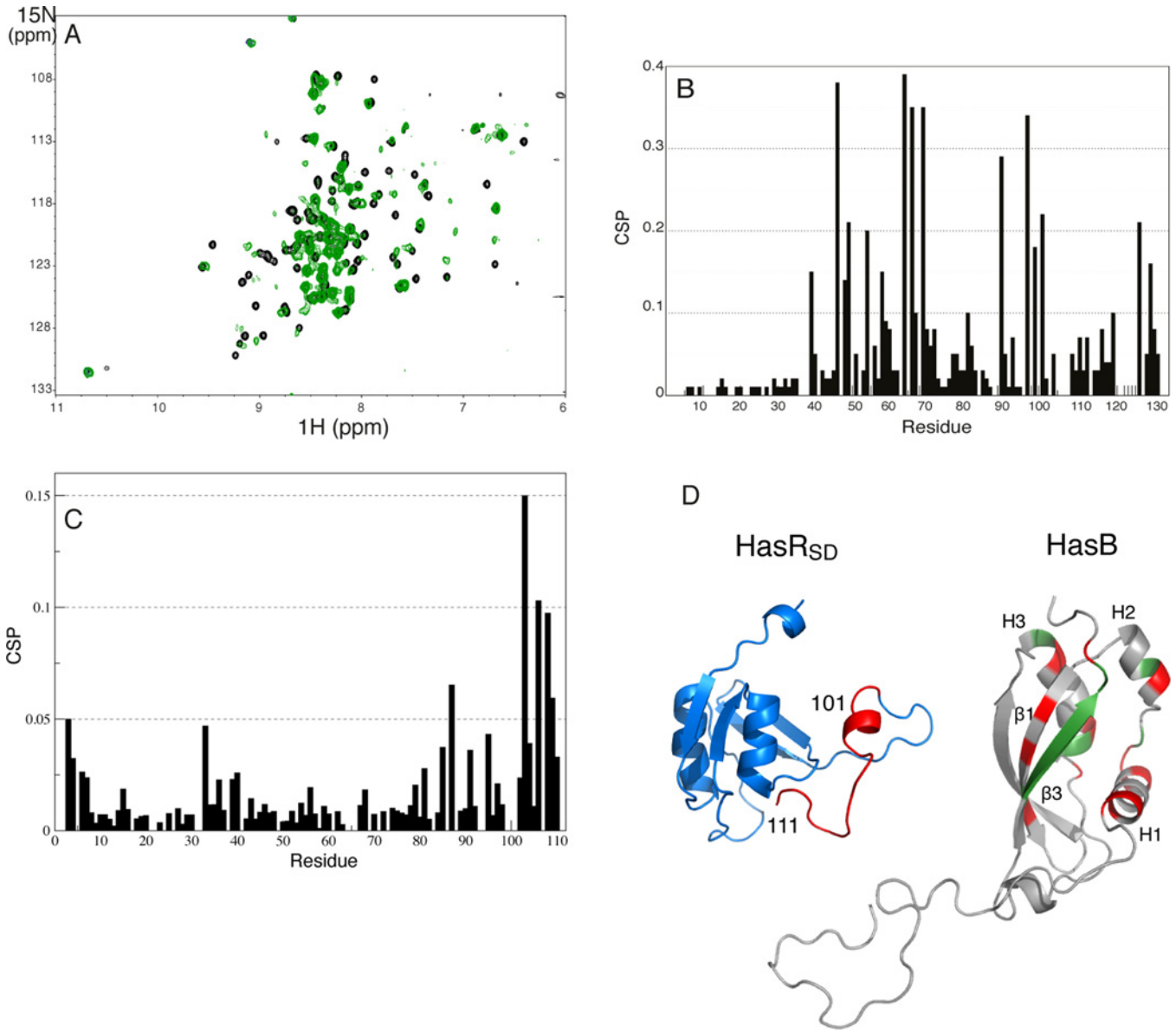

Figure 6 HasB–HasR$_{SD}$ interaction

(**A**) ^{15}N–^{1}H HSQC spectra of HasB alone (black) or in the presence of HasR$_{SD}$ (green). (**B**) CSP values of HasB residues upon HasR$_{SD}$ binding. (**C**) CSP values of HasR$_{SD}$ residues upon HasB binding. (**D**) CSPs mapped on to HasB (right) and HasR$_{SD}$ structures (left). Residues with the highest CSP values are shown in red, those experiencing conformation exchange are shown in green.

is that of FpvA [40]. As shown in Figure 3, in this structure the signalling domain and the barrel are very close and interact together. Secondly, the distance between the signalling domain and the barrel of HasR is shortened in the loaded form, thus the signalling domain appears to come closer to the barrel, when signalling activators are present (Figure 3). This change in distance occurring upon the arrival of signalling activators could be an integral part of the signalling process.

Our NMR results show that the presence of signalling activators also induces local conformational changes of some residues in the linker (91–93 and 101–109) and in the two helices (H1 and H2) of the signalling domain (Figure 5). Such changes might increase the likelihood of HasR's interaction with its partners. Indeed, we have previously shown that the linker interacts with HasB and these two helices recognize the anti-sigma factor HasS, the regulator of the sigma factor, ECFσ, that induces the expression of the *has* operon [15].

These local structural changes of the linker and of the signalling domain are similar to the results of an EPR study on the ferric citrate transporter (FecA) [41]. In the present study, the substrate binding did not modify either the overall structure of the signalling domain or its dynamics. Similar to HasR, only some local conformational changes were detected in the FecA signalling domain upon ferric citrate binding. However, neither the exact position of the signalling domain nor its distance from the barrel has been defined to date.

In the case of the X-ray structure of FpvA (PDB code 2O5P), the linker containing the region interacting with TonB is folded inside the barrel and thus inaccessible [40]. Moreover, as stated above, the signalling domain of FpvA interacts with its barrel (Figure 3),

making the interaction with a globular protein such as TonB sterically impossible. The authors proposed that the signalling domain must move away to allow TonB–linker interaction. Since the FpvA linker (33 residues) is longer than that of HasR (27 residues), the compactness of the linker in the FpvA structure might have resulted from the crystal packing.

To gain insight into further steps of the signalling, we analysed the complex between HasR–haem–HasA and HasB by NMR. In this complex, the intensity of the resonances belonging to the signalling domain and the linker decreases dramatically, indicating either conformational change of these regions and/or a reduction in the overall tumbling rates due to the interaction. Previously, we studied by NMR the formation of a complex between HasB and a peptide that corresponded to the linker and showed that the linker peptide, which was disordered while alone, formed an inter-protein β-sheet with the third β-strand of HasB [12]. In the present study, we show that HasB interacts with $HasR_{SD}$ (the signalling domain plus the linker) and the full-length HasR. Our data agree well with the formation of an inter-protein β-sheet between the linker and HasB in the context of the whole HasR. The interaction between HasB and HasR via the linker explains the reduction in the overall dynamics of the signalling domain. Furthermore, local conformational changes detected in the β-sheet (73–75, 77 and 82–85) of the signalling domain just upstream of the linker might result from this inter-protein β-sheet formation (Figure 5).

The structural basis of the signalling through a TonB-dependent system is not well understood. Our data on the Has system led us to propose the following model of the signalling process. The signalling domain and the linker containing the HasB box are highly flexible during the two first stages of the process, i.e. when the transporter is free and when the signalling activators are present. Furthermore, the signalling domain is positioned far away from the β-barrel, in the periplasmic space. The dynamics and the positions of the signalling domain and the linker, as well as their local conformational changes induced by the presence of signalling activators would favour the interaction with their partners, i.e. HasB and the anti-sigma factor HasS. Once the linker is trapped by HasB, the formation of the inter-protein β-sheet stabilizes the position of the signalling domain, which would promote or stabilize its interaction with HasS. The latter is attached to the cytoplasmic membrane and recognizes the signalling domain via its periplasmic region, which is partially disordered and has an elongated shape [7,15]. These structural features of HasS and the location of the signalling domain towards the cytoplasmic membrane would favour the likelihood of their interaction and thus the signal transfer between the two membranes.

The present study provides essential elements to clarify the signalling from the OM transporter to its cytoplasmic membrane partners. To unravel the next steps of signalling, further investigation with the whole multi-protein complexes in a membrane mimicking environment would be crucial.

AUTHOR CONTRIBUTION

Halina Wojtowicz, Gisele Cardoso de Amorim, Idir Malki, Catherine Simenel and Philippe Delepelaire prepared samples and carried out experiments. Gérard Pehau-Arnaudet and Francesca Gubellini assisted in EM sample preparation and data collection. Halina Wojtowicz, Ada Prochnicka-Chalufour and Rémi Fronzes analysed the EM data and performed the modelling. Javier Perez performed SAXS experiments and supervised analysis. Olga Roudenko and Alexandros Koutsioubas performed modelling from the SAXS data. Ada Prochnicka-Chalufour and Philippe Delepelaire edited and reviewed the paper before submission. Nadia Izadi-Pruneyre and Muriel Delepierre provided resources. Nadia Izadi-Pruneyre designed, co-ordinated the study and wrote the paper with the input from all authors.

ACKNOWLEDGEMENTS

We thank Emmanuel Frachon, from the Platform of Recombinant Protein of the Institut Pasteur, for bacterial cell production. We thank Dominique Durand and Patrice Vachette for the first SAXS measurements on HasR. We thank Florence Cordier and Bertrand Raynal for helpful discussions.

FUNDING

This work was funded by the Institut Pasteur, the Centre National de la Recherche Scientifique (CNRS), two grants from the ANR (Agence Nationale de la Recherche) [grant numbers HEMESTOCKEXCHANGE 12-BSV3-0022-01 and HEMETRANS 08-BLAN-0160]; Equipement d'Excellence CACSICE and SOLEIL [grant number 2013448]. H.W. was funded by postdoctoral fellowships from the Mairie de Paris [grant number 2012-209].

REFERENCES

1 Lamont, I.L., Beare, P.A., Ochsner, U., Vasil, A.I. and Vasil, M.L. (2002) Siderophore-mediated signaling regulates virulence factor production in Pseudomonas aeruginosa. Proc. Natl. Acad. Sci. U.S.A. **99**, 7072–7077 CrossRef PubMed
2 Braun, V., Mahren, S. and Sauter, A. (2006) Gene regulation by transmembrane signaling. BioMetals **19**, 103–113 CrossRef PubMed
3 Brooks, B.E. and Buchanan, S.K. (2008) Signaling mechanisms for activation of extracytoplasmic function (ECF) sigma factors. Biochim. Biophys. Acta **1778**, 1930–1945 CrossRef PubMed
4 Mascher, T. (2013) Signaling diversity and evolution of extracytoplasmic function (ECF) sigma factors. Curr. Opin. Microbiol. **16**, 148–155 CrossRef PubMed
5 Rossi, M.S., Paquelin, A., Ghigo, J.M. and Wandersman, C. (2003) Haemophore-mediated signal transduction across the bacterial cell envelope in Serratia marcescens: the inducer and the transported substrate are different molecules. Mol. Microbiol. **48**, 1467–1480 CrossRef PubMed
6 Ghigo, J.M., Letoffe, S. and Wandersman, C. (1997) A new type of hemophore-dependent heme acquisition system of Serratia marcescens reconstituted in Escherichia coli. J. Bacteriol. **179**, 3572–3579 PubMed
7 Izadi-Pruneyre, N., Wolff, N., Delepierre, M. and Lecroisey, A. (2011) Hemophore HasA. Encyclopedia of Inorganic and Bioinorganic Chemistry, John Wiley & Sons, Ltd, USA
8 Izadi-Pruneyre, N., Huche, F., Lukat-Rodgers, G.S., Lecroisey, A., Gilli, R., Rodgers, K.R., Wandersman, C. and Delepelaire, P. (2006) The heme transfer from the soluble HasA hemophore to its membrane-bound receptor HasR is driven by protein-protein interaction from a high to a lower affinity binding site. J. Biol. Chem. **281**, 25541–25550 CrossRef PubMed
9 Cwerman, H., Wandersman, C. and Biville, F. (2006) Heme and a five-amino-acid hemophore region form the bipartite stimulus triggering the has signaling cascade. J. Bacteriol. **188**, 3357–3364 CrossRef PubMed
10 Wandersman, C. and Delepelaire, P. (2012) Haemophore functions revisited. Mol. Microbiol. **85**, 618–631 CrossRef PubMed
11 Krieg, S., Huche, F., Diederichs, K., Izadi-Pruneyre, N., Lecroisey, A., Wandersman, C., Delepelaire, P. and Welte, W. (2009) Heme uptake across the outer membrane as revealed by crystal structures of the receptor-hemophore complex. Proc. Natl. Acad. Sci. U.S.A. **106**, 1045–1050 CrossRef PubMed
12 de Amorim, G.C., Prochnicka-Chalufour, A., Delepelaire, P., Lefevre, J., Simenel, C., Wandersman, C., Delepierre, M. and Izadi-Pruneyre, N. (2013) The structure of HasB reveals a new class of TonB protein fold. PLoS One **8**, e58964 CrossRef PubMed
13 Garcia-Herrero, A. and Vogel, H.J. (2005) Nuclear magnetic resonance solution structure of the periplasmic signalling domain of the TonB-dependent outer membrane transporter FecA from Escherichia coli. Mol. Microbiol. **58**, 1226–1237 CrossRef PubMed
14 Ferguson, A.D., Amezcua, C.A., Halabi, N.M., Chelliah, Y., Rosen, M.K., Ranganathan, R. and Deisenhofer, J. (2007) Signal transduction pathway of TonB-dependent transporters. Proc. Natl. Acad. Sci. U.S.A. **104**, 513–518 CrossRef PubMed
15 Malki, I., Simenel, C., Wojtowicz, H., de Amorim, G.C., Prochnicka-Chalufour, A., Hoos, S., Raynal, B., England, P., Chaffotte, A., Delepierre, M. et al. (2014) Interaction of a partially disordered antisigma factor with its partner, the signaling domain of the TonB-dependent transporter HasR. PLoS One **9**, e89502 CrossRef PubMed
16 Huche, F., Delepelaire, P., Wandersman, C. and Welte, W. (2006) Purification, crystallization and preliminary X-ray analysis of the outer membrane complex HasA-HasR from Serratia marcescens. Acta Crystallogr. Sect. F Struct. Biol. Cryst. Commun. **62**, 56–60 CrossRef PubMed

17 Czjzek, M., Letoffe, S., Wandersman, C., Delepierre, M., Lecroisey, A. and Izadi-Pruneyre, N. (2007) The crystal structure of the secreted dimeric form of the hemophore HasA reveals a domain swapping with an exchanged heme ligand. J. Mol. Biol. **365**, 1176–1186 CrossRef PubMed

18 Malki, I., Cardoso de Amorim, G., Simenel, C., Prochnicka-Chalufour, A., Delepierre, M. and Izadi-Pruneyre, N. (2013) (1)H, (13)C and (15)N resonance assignments of the periplasmic signalling domain of HasR, a TonB-dependent outer membrane heme transporter. Biomol. NMR Assign. **7**, 43–46 CrossRef PubMed

19 Lefevre, J., Simenel, C., Delepelaire, P., Delepierre, M. and Izadi-Pruneyre, N. (2007) (1)H, (13)C and (15)N resonance assignments of the C-terminal domain of HasB, a specific TonB like protein, from Serratia marcescens. Biomol. NMR Assign. **1**, 197–199 CrossRef PubMed

20 Lefevre, J., Delepelaire, P., Delepierre, M. and Izadi-Pruneyre, N. (2008) Modulation by substrates of the interaction between the HasR outer membrane receptor and its specific TonB-like protein, HasB. J. Mol. Biol. **378**, 840–851 CrossRef PubMed

21 Caillet-Saguy, C., Piccioli, M., Turano, P., Izadi-Pruneyre, N., Delepierre, M., Bertini, I. and Lecroisey, A. (2009) Mapping the interaction between the hemophore HasA and its outer membrane receptor HasR using CRINEPT-TROSY NMR spectroscopy. J. Am. Chem. Soc. **131**, 1736–1744 CrossRef PubMed

22 Delaglio, F., Grzesiek, S., Vuister, G.W., Zhu, G., Pfeifer, J. and Bax, A. (1995) NMRPipe: a multidimensional spectral processing system based on UNIX pipes. J. Biomol. NMR **6**, 277–293 CrossRef PubMed

23 Vranken, W.F., Boucher, W., Stevens, T.J., Fogh, R.H., Pajon, A., Llinas, M., Ulrich, E.L., Markley, J.L., Ionides, J. and Laue, E.D. (2005) The CCPN data model for NMR spectroscopy: development of a software pipeline. Proteins **59**, 687–696 CrossRef PubMed

24 Krzeminski, M., Loth, K., Boelens, R. and Bonvin, A.M. (2010) SAMPLEX: automatic mapping of perturbed and unperturbed regions of proteins and complexes. BMC Bioinformatics **11**, 51 CrossRef PubMed

25 Zoonens, M., Catoire, L.J., Giusti, F. and Popot, J.L. (2005) NMR study of a membrane protein in detergent-free aqueous solution. Proc. Natl. Acad. Sci. U.S.A. **102**, 8893–8898 CrossRef PubMed

26 Tang, G., Peng, L., Baldwin, P.R., Mann, D.S., Jiang, W., Rees, I. and Ludtke, S.J. (2007) EMAN2: an extensible image processing suite for electron microscopy. J. Struct. Biol. **157**, 38–46 CrossRef PubMed

27 Scheres, S.H. (2012) A Bayesian view on cryo-EM structure determination. J. Mol. Biol. **415**, 406–418 CrossRef PubMed

28 Scheres, S.H. (2015) Semi-automated selection of cryo-EM particles in RELION-1.3. J. Struct. Biol. **189**, 114–122 CrossRef PubMed

29 Althoff, T., Mills, D.J., Popot, J.L. and Kuhlbrandt, W. (2011) Arrangement of electron transport chain components in bovine mitochondrial supercomplex I1III2IV1. EMBO J. **30**, 4652–4664 CrossRef PubMed

30 le Maire, M., Champeil, P. and Moller, J.V. (2000) Interaction of membrane proteins and lipids with solubilizing detergents. Biochim. Biophys. Acta **1508**, 86–111 CrossRef PubMed

31 Pettersen, E.F., Goddard, T.D., Huang, C.C., Couch, G.S., Greenblatt, D.M., Meng, E.C. and Ferrin, T.E. (2004) UCSF Chimera–a visualization system for exploratory research and analysis. J. Comput. Chem. **25**, 1605–1612 CrossRef PubMed

32 Sali, A. and Blundell, T.L. (1993) Comparative protein modelling by satisfaction of spatial restraints. J. Mol. Biol. **234**, 779–815 CrossRef PubMed

33 Berthaud, A., Manzi, J., Perez, J. and Mangenot, S. (2012) Modeling detergent organization around aquaporin-0 using small-angle X-ray scattering. J. Am. Chem. Soc. **134**, 10080–10088 CrossRef PubMed

34 Perez, J. and Koutsioubas, A. (2015) Memprot: a program to model the detergent corona around a membrane protein based on SEC-SAXS data. Acta Crystallogr. D Biol. Crystallogr. **71**, 86–93 CrossRef PubMed

35 Evrard, G., Mareuil, F., Bontems, F., Sizun, C. and Perez, J. (2011) DADIMODO: a program for refining the structure of multidomain proteins and complexes against small-angle scattering data and NMR-derived restraints. J. Appl. Crystallogr. **44**, 1264–1271 CrossRef

36 Svergun, D., Barberato, C. and Koch, M.H.J. (1995) CRYSOL – a program to evaluate X-ray solution scattering of biological macromolecules from atomic coordinates. J. Appl. Crystallogr. **28**, 768–773 CrossRef

37 Hinsen, K. (2000) The molecular modeling toolkit: a new approach to molecular simulations. J. Comput. Chem. **21**, 79–85 CrossRef

38 Noinaj, N., Guillier, M., Barnard, T.J. and Buchanan, S.K. (2010) TonB-dependent transporters: regulation, structure, and function. Annu. Rev. Microbiol. **64**, 43–60 CrossRef PubMed

39 Krewulak, K.D. and Vogel, H.J. (2011) TonB or not TonB: is that the question? Biochem. Cell Biol. **89**, 87–97 PubMed

40 Brillet, K., Journet, L., Celia, H., Paulus, L., Stahl, A., Pattus, F. and Cobessi, D. (2007) A beta strand lock exchange for signal transduction in TonB-dependent transducers on the basis of a common structural motif. Structure **15**, 1383–1391 CrossRef PubMed

41 Mokdad, A., Herrick, D.Z., Kahn, A.K., Andrews, E., Kim, M. and Cafiso, D.S. (2012) Ligand-induced structural changes in the Escherichia coli ferric citrate transporter reveal modes for regulating protein-protein interactions. J. Mol. Biol. **423**, 818–830 CrossRef PubMed

Received 18 February 2016/9 May 2016; accepted 13 May 2016
Accepted Manuscript online 23 May 2016, doi:10.1042/BCJ20160131